Available online at www.sciencedirect.com
ScienceDirect
Journal of Power Sources 175 (2008) 106–119
JOURNAL OF POWER SOURCES
www.elsevier.com/locate/jpowsour

Effects of electrode wettabilities on liquid water behaviours in PEM fuel cell cathode

Kui Jiao, Biao Zhou *

Department of Mechanical, Automotive & Materials Engineering, University of Windsor, ON, Canada, N9B 3P4

Received 14 June 2007; received in revised form 11 September 2007; accepted 12 September 2007
Available online 21 September 2007

Abstract

Liquid water transport is one of the key challenges for water management in a proton exchange membrane (PEM) fuel cell. Investigation of the air–water flow patterns inside fuel cell gas flow channels with gas diffusion layer (GDL) would provide valuable information that could be used in fuel cell design and optimization. This paper presents numerical investigations of air–water flow across an innovative GDL with catalyst layer and serpentine channel on PEM fuel cell cathode by use of a commercial Computational Fluid Dynamics (CFD) software package FLUENT. Different static contact angles (hydrophilic or hydrophobic) were applied to the electrode (GDL and catalyst layer). The results showed that different wettabilities of cathode electrode could affect liquid water flow patterns significantly, thus influencing on the performance of PEM fuel cells. The detailed flow patterns of liquid water were shown, several gas flow problems were observed, and some useful suggestions were given through investigating the flow patterns.

Keywords: Water management; Wettability; Static contact angle; Gas diffusion layer (GDL); CFD; FLUENT

1. Introduction

Low operating temperature and zero/low emissions have made Proton Exchange Membrane (PEM) fuel cells become the most promising power source of the future [1]. However, to achieve commercialization, the performance of PEM fuel cells needs to be improved by proper engineering design and optimization. Due to the special chemical structure of the PEM, the membrane must be well hydrated to ensure that a sufficient amount of hydrogen ions could cross. On the other hand, due to the low operating temperature of PEM fuel cells (30–100 °C) [1], excessive humidification could result in water vapour condensation that could subsequently block the gas flow channels resulting in a lower air flow rate on the cathode side, thus decreasing fuel cell performance. Water content is also an important factor that affects the ohmic resistance in the membrane [2]. Therefore, keeping an appropriate amount of water content in the fuel cell to avoid both membrane dehydration and water vapour condensation has been a critical issue in improving fuel cell performance. In reality, however, it is almost impossible to manage water on both the anode and cathode sides without dehydration and condensation; this is simply because water vapour condensation in the gas flow channels of practical fuel cell applications is unavoidable [2]. Therefore, water management, to which many engineers and scientists have recently paid particular attention, has been a critical challenge for a high-performance fuel cell design and optimization. Wang [3] made a comprehensive review of water management in fuel cells, and Kraytsberg and Ein-Eli [4] also identified different kinds of water management related issues.

In the last decade, water management related studies were performed numerically and experimentally for different purposes and in several ways. A CFD modeling of PEM fuel cells which simultaneously considered the electrochemical kinetics, current distributions, hydrodynamics, and multi-component transport was conducted by Um et al. [5]. A three-dimensional (3D) numerical simulation of a straight gas flow channel in a PEM fuel cell was performed by Dutta et al. [6] using a commercial CFD software FLUENT. Hontanon et al. [7] also employed

* Corresponding author. Tel.: +1 519 253 3000x2630; fax: +1 519 973 7007.
E-mail address: bzhou@uwindsor.ca (B. Zhou).

0378-7753/$ – see front matter © 2007 Elsevier B.V. All rights reserved.
doi:10.1016/j.jpowsour.2007.09.048

FLUENT to implement their 3D, stationary gas flow model. A study exploring the steady-state gas transport phenomena in micro-scale parallel flow channels was conducted by Cha et al. [8] in which oxygen concentration along a single gas flow channel and other flow patterns that may affect fuel cell performance were discussed. Similarly, gas concentration of a steady-state flow along fuel cell flow channels was obtained numerically by Kulikovsky [9]. However, in all the studies mentioned above, the effects of liquid water were neglected. Yi et al. [2] pointed out that water vapour condensation was inevitable on both the anode and cathode sides of a PEM fuel cell, and they discussed a liquid water removal technique that used a water transport plate to lead excess liquid water to the coolant flow channels by a pressure difference. Wang et al. [10] conducted a two-phase model on PEM fuel cell cathode to address the liquid water concentrations. You and Liu [11] also considered liquid water concentration in a straight channel on the cathode side. Both the references [10,11] showed the importance for considering liquid water in numerical modeling of PEM fuel cells. He et al. [12] conducted a two-phase, two-dimensional numerical model for PEM fuel cell cathode with interdigitated flow channels. A numerical simulation considering water management for PEM fuel cell catalyst layer was performed by Wang et al. [13]. An analysis of proton and water transport was performed by Carnes and Djilali [14] by using the binary friction membrane model. Effects of humidification on cathode liquid water condensation were studied by Lee and Chu [15] by using their 3D numerical model. A two-phase, two-dimensional, non-isothermal numerical model was conducted by Meng [16] to investigate both condensation and evaporation of water in PEM fuel cell. In addition, more

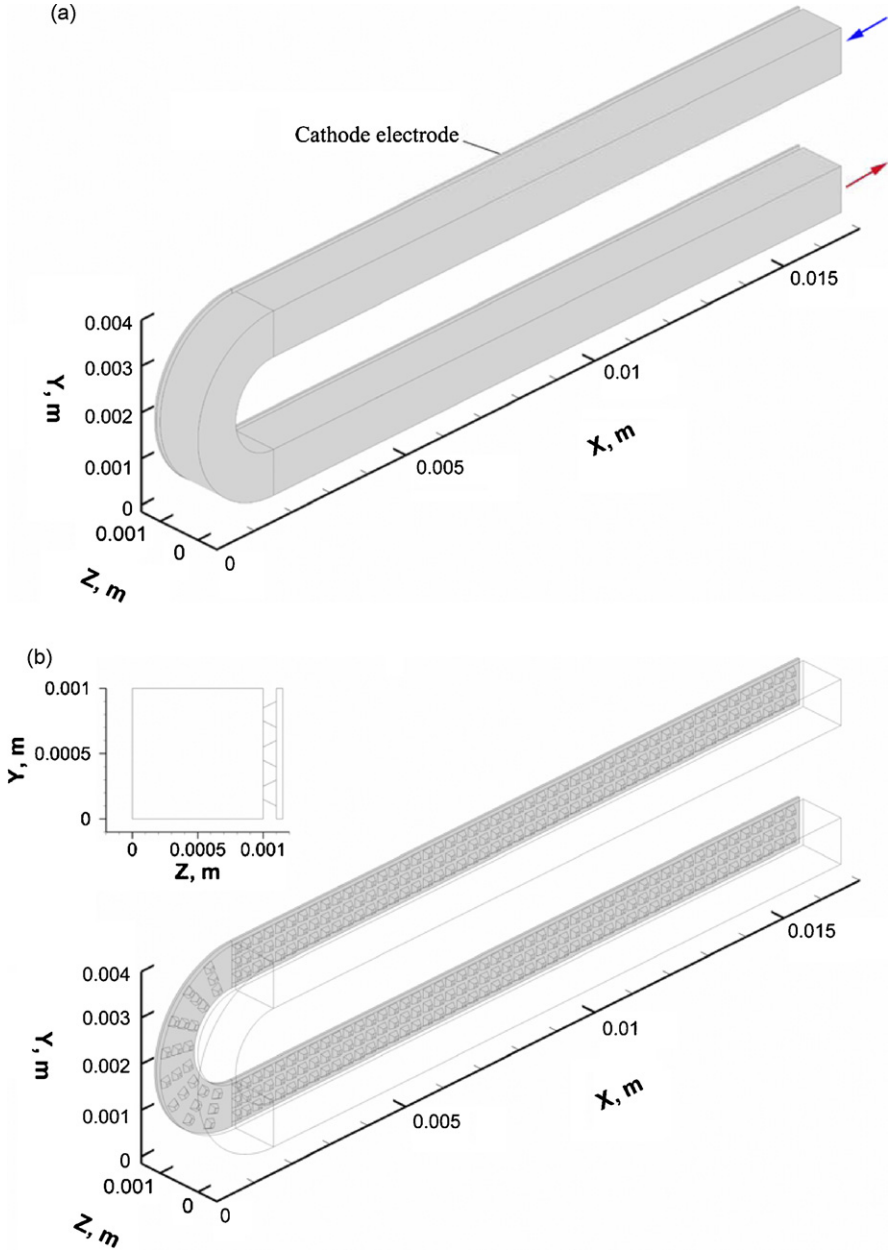

Fig. 1. Computation domain ((a) general view; (b) structure of the GDL).

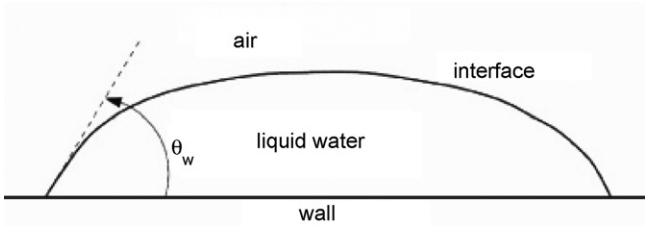

Fig. 2. Measuring the contact angle.

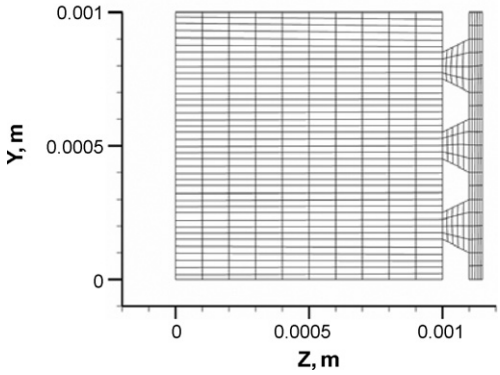

Fig. 3. Mesh on y–z plane.

two-phase models have also been published [17–19], these simulations predicted water flooding inside PEM fuel cells, and the liquid water effects on PEM fuel cell performances. Large-scale simulations for complex flow field were also performed with experimental validations [20–23], these simulations provided more realistic results rather than considering one single cell.

By far, to the authors' knowledge, most of the two-phase numerical models have not considered the interface tracking between liquid water and gas. The detailed behaviours of liquid water transport inside PEM fuel cells were rarely discussed except for the present authors' previous study [24], which only dealt with part of serpentine channels—the single U-shaped channel. Recently, the authors also conducted two more studies that dealt with liquid water in serpentine and straight parallel fuel cell stacks [25,26].

Experimental studies related to water management were also performed by different research groups. Nguyen and Knobbe [27] developed a liquid water management strategy for PEM fuel cell stacks. Neutron radiography method was used by Trabold et al. [28] to investigate water transport in PEM fuel cell. Li et al. [29] also used neutron imaging technique to help their flow channel design. A transparent single-serpentine PEM fuel cell was built by Spernjak et al. [30] to investigate liquid water formation and transport.

On the cathode side of fuel cells, most of the water, which is mainly produced by the electrochemical reaction, flows through the gas diffusion layer (GDL) to the gas flow channels. Therefore, liquid water flow across these porous media to the gas flow channels, and formation of water droplets during this process are both unavoidable and important for practical operations of PEM fuel cells. As the authors reviewed, experimental studies to probe detailed liquid water transport from the GDL into the gas flow channels have been performed by Yang et al. [31] and Zhang et al. [32]. In these studies, the observations of liquid water distributions on the GDL surfaces were made in a transparent PEM fuel cell, and liquid water droplet formation and emerging of liquid water were discussed. Numerical models that considered the porous media were developed in several ways. Nam and Kaviany [33] developed a two dimensional, two-phase numerical model by considering random carbon fibre mats as the GDL. Single- and two-layer diffusion media were both considered to investigate the effective diffusivity and water saturation. A study on the interaction between the GDL and the flow field was performed by Dohle et al. [34] numerically and experimentally. Other models that considered the porous media also mainly focused on the porosity of the carbon fibre paper that could influence the performances of PEM fuel cells [35,36]. However, the detailed flow patterns that liquid water exhibits across the porous medium and the effects of the micro-structures of GDL were rarely discussed.

Some very important facts have often not been paid serious attention: the conventional GDLs are not effective for water removal. This is because the micro-structure and the size of the pores of conventional GDLs are very arbitrary, and the sizes of the pores are very small (10 and 30 μm). Due to the physical features of the conventional GDLs, it is very frequent for liquid water to flood the GDL and catalyst layer in practical PEM

Table 1
Three simulated cases

Case no.	Static contact angle	Inlet velocity ($m\,s^{-1}$)	Initial film thickness (mm)	Initial water amount (mm^3)	Initial water distribution	Corresponding PEM fuel cell operating condition
1	45° (hydrophilic) for GDL	10	0.03	1.04	Water films with a thickness of 0.03 mm placed on catalyst layer	Water flooding for case with proposed hydrophilic GDL
2	135° (hydrophobic) for GDL	10	0.03	1.04	Water films with a thickness of 0.03 mm placed on catalyst layer	Water flooding for case with proposed hydrophobic GDL
3	135° (hydrophobic) for GDL and catalyst layer	10	0.03	1.04	Water films with a thickness of 0.03 mm placed on catalyst layer	Water flooding for case with proposed hydrophobic GDL and hydrophobic catalyst layer

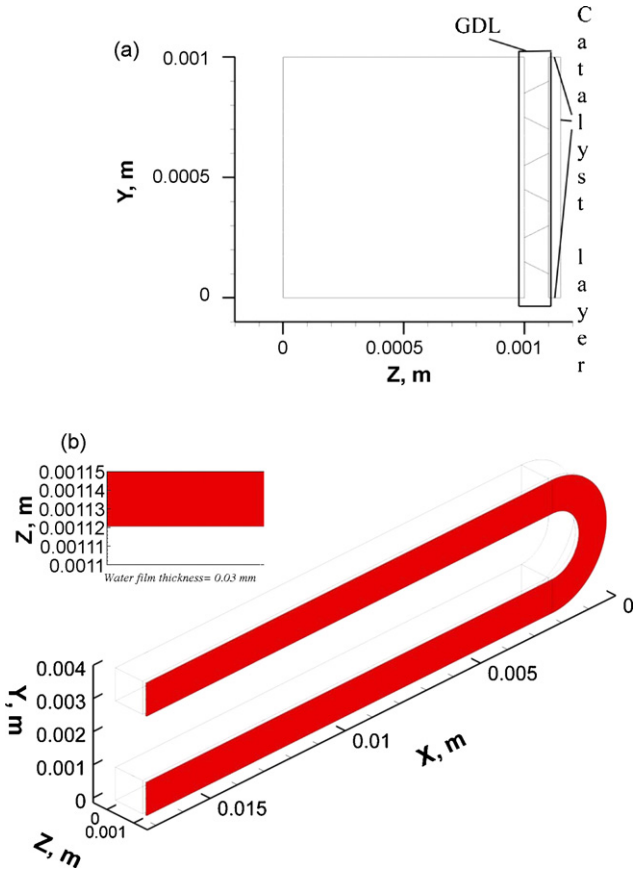

Fig. 4. Electrode surfaces and initial water condition ((a) surfaces of the GDL and catalyst layer; (b) initial water distribution).

fuel cells. The main reason causing frequent flooding is that the arbitrary structure of conventional GDLs does not allow a well-organized liquid water flow.

In the authors' previous study [37], a unit serpentine gas flow channel with three different kinds of micro-structures of innovative GDLs were studied, and it was concluded that one of the three GDLs performed the best water removing ability. In this paper, the wettability of the best GDL in reference [37] was studied; different static contact angles (hydrophobic, hydrophilic) were assigned to the electrode (GDL and catalyst layer). In this work, the details of phase change and electro-chemical reaction were not considered. Based on the authors' understanding, the effect of the electro-chemical reaction inside the PEM fuel cell on liquid water behaviour is mainly to continuously supply water. Based on this premise, various operating conditions for a PEM fuel cell could be simulated without involving details of electro-chemical reactions. In the present work, therefore, an initial liquid water distribution was employed to simplify the complex process of real PEM fuel cell operating condition.

In the following, the computation domain, solution procedure and mesh independency are introduced. Then the results and discussions are presented. Finally, conclusions are drawn and some valuable design and optimization related suggestions are given.

2. Numerical model setup

2.1. Computation domain with innovative micro-flow-channels of GDL, and boundary conditions

Fig. 1 illustrates the schematics of the computation domain. At the top left side of Fig. 1b, the cross-section (the y–z plane) along the center-plane of the GDL holes was shown. The com-

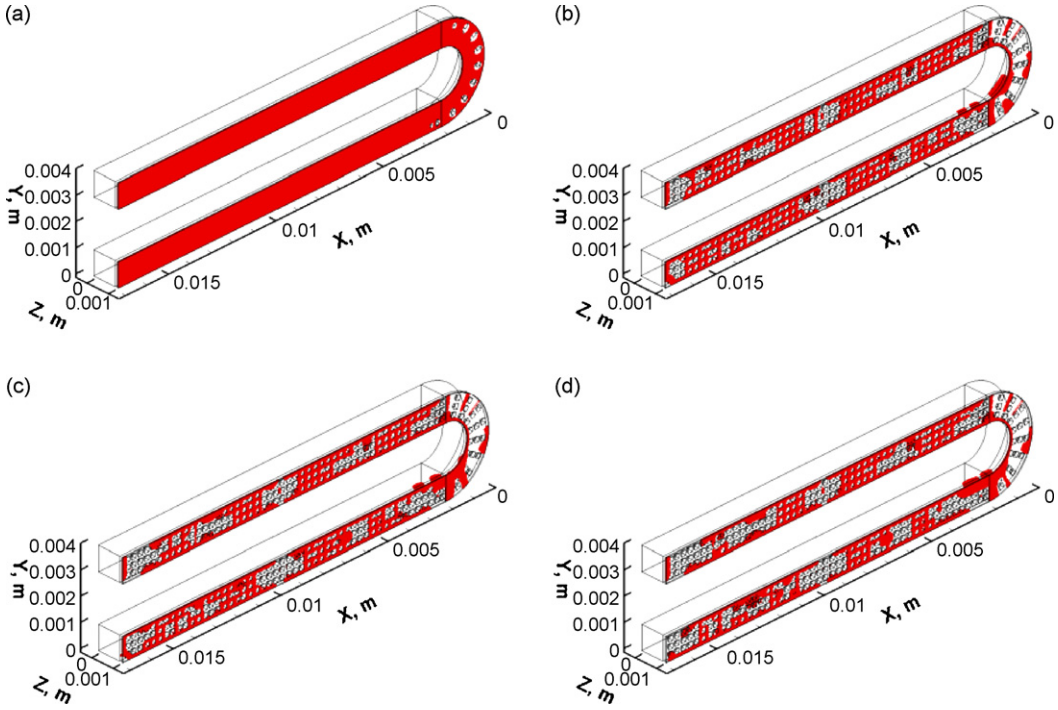

Fig. 5. Liquid water distribution in 3D view for Case 1 ((a) $t = 0.0002$ s; (b) $t = 0.01$ s; (c) $t = 0.015$ s; (d) $t = 0.02$ s).

putation domain consists of the U-shaped channel—the unit of a serpentine PEM fuel cell flow channel and the cathode electrode. The gas flow channel has a cross-section of 1 mm × 1 mm along the y- and z-directions. Each straight section of the gas flow channel is 15 mm long. On the cathode electrode, small paths are used to represent the holes on the GDL: trapezoids with the height of 0.1 mm along the z-direction, and the minimum area (0.1 mm × 0.1 mm along the x- and y- directions) facing the gas flow channel.

As mentioned in the introduction, the conventional GDLs are not effective for water removal due to the random nature of its micro-structure and small pore size (10–30 μm). Therefore, the innovative micro-structure of the GDL is studied, all the "pores" are well designed and structured, i.e., well-structured small holes (micro-flow-channels) connecting the gas flow channel and catalyst layer as shown in Fig. 1b. Furthermore there is a gap of 0.05 mm between the GDL and the membrane. The purpose of this study is to investigate how the liquid water flows through the GDL into the gas flow channel, to simplify the numerical model, the gap between the GDL and the membrane were set to have unity porosity.

The isothermal air–water transport process inside the computation domain was modeled as a 3D two-phase viscous laminar flow. A no-slip boundary condition was applied to the surrounding walls. A velocity inlet boundary condition (uniform air velocity distribution of 10 m s^{-1} with a direction normal to the inlet boundary) was applied at the air inlet of the upper section of the U-shaped channel. At the outlet, the boundary condition was assigned as outlet flow (the gradients of all flow properties are zero). Gravity was taken as being along the negative y-direction. To simulate water removal characteristics of the GDL, different static contact angels were assigned to the electrode and an initial water distribution inside the computation domain was carefully set up, and the details are given in the "results and discussions" section.

2.2. Computational methodology

The numerical simulations of the 3D, unsteady, laminar, two-phase flow in the computation domain was performed using FLUENT [38]. An inspection of the numerical setup revealed that the Reynolds number in the model was less than 700, thereby verifying laminar flow assumption. No energy equations were considered thus the conservation of mass and momentum were the governing equations for the model. To track the air–water two-phase flow interface inside the computation domain, the Volume-Of-Fluid (VOF) [38] method implemented in FLUENT was used. The VOF model is designed for two or more immiscible fluids, where the position of the interface between fluids is of interest.

Then the conservation laws of mass and momentum governing the unsteady, laminar flow could be written as [38]:

Continuity equation:

$$\frac{\partial \rho}{\partial t} + \nabla \cdot (\rho \vec{v}) = 0 \tag{1}$$

Momentum equation:

$$\frac{\partial (\rho \vec{v})}{\partial t} + \nabla \cdot (\rho \vec{v} \vec{v}) = -\nabla p + \nabla \cdot [\mu (\nabla \vec{v} + \nabla \vec{v}^T)] + \rho g + \vec{F} \tag{2}$$

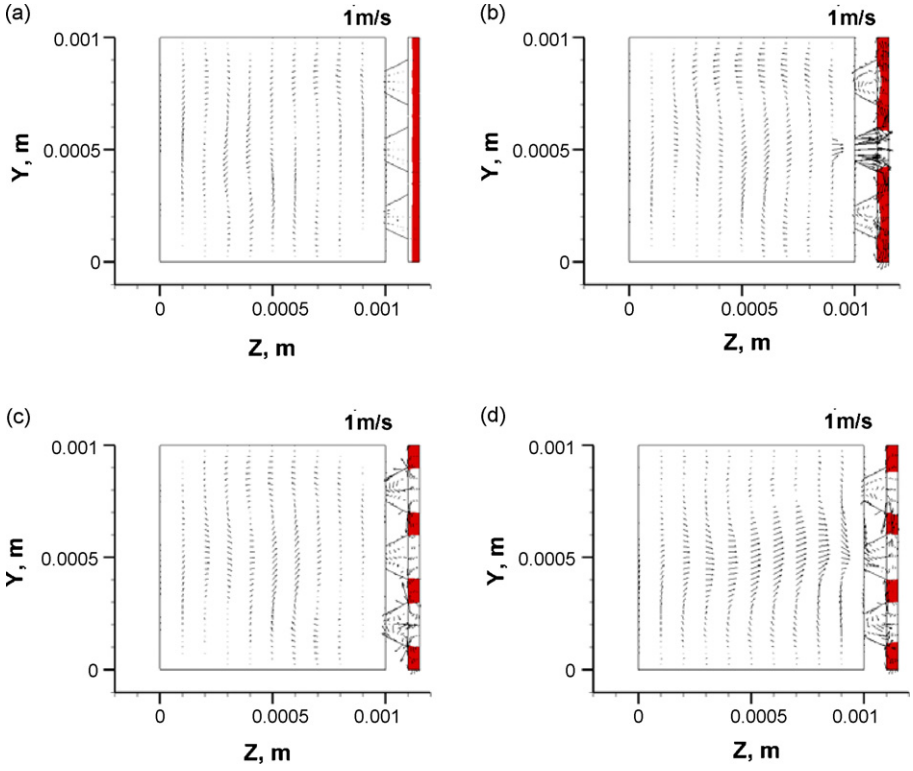

Fig. 6. Water distribution and velocity field on the plane at $x = 0.00805$ m in outlet section for Case 1 ((a) $t = 0.001$ s; (b) $t = 0.0015$ s; (c) $t = 0.002$ s; (d) $t = 0.02$ s).

where p is the static pressure and $\vec{F}$ is the surface tension force.

For volume fraction of liquid water (α_2):

$$\frac{\partial \alpha_2}{\partial t} + \vec{v} \cdot \nabla \alpha_2 = 0 \quad (3)$$

The volume fraction of air (α_1) could be obtained based on the following relationship:

$$\alpha_1 + \alpha_2 = 1 \quad (4)$$

All the other properties (e.g., viscosity) could be computed in a volume-fraction weighted-average manner as:

$$\mu = \alpha_2 \mu_2 + (1 - \alpha_2)\mu_1 \quad (5)$$

In the FLUENT simulation package, the surface tension is considered as a source term in the momentum equation. For two-phase flow, it can be expressed as:

$$F_{\text{vol}} = \sigma_{12} \frac{\rho \kappa \nabla \alpha_1}{1/(2(\rho_1 + \rho_2))} \quad (6)$$

where F_{vol} is the source term of the surface tension in momentum equation, σ_{12} the surface tension coefficient, ρ the volume-averaged density, and κ is the surface curvature at the interface between two phases. The surface curvature can be expressed as:

$$\kappa = \nabla \cdot \hat{n} = \nabla \cdot (\hat{n}_{\text{w}} \cos \theta_{\text{w}} + \hat{t}_{\text{w}} \sin \theta_{\text{w}}) \quad (7)$$

where $\hat{n}$ is the unit vector normal to the interface between two phases near the walls, $\hat{n}_{\text{w}}$ the unit vector normal to the walls, $\hat{t}_{\text{w}}$ the unit vector tangential to the walls, and θ_{w} is the static contact angle at the walls, as shown in Fig. 2. For the electrode surfaces with different wettabilities, different static contact angles were assigned, and different contact angles could result in different surface tensions (F_{vol}), thus influencing on water transport.

2.3. Validation of grid independency

There were 622,620 cells meshed in the computation domain. Fig. 3 shows the mesh on y–z plane for the computation domain. Each cell in the straight channel sections had the same size with dimensions of $0.025 \times 0.025 \times 0.1$. Trapeziform cells were employed to generate the corners of the serpentine gas flow channels. The GDL holes were divided into four sections along the x- and y-directions, and five sections along the z-direction. The dimensions of the cells along the z-direction are 0.02 and 0.01 mm for the GDL and the catalyst layer, respectively. This computation domain was first studied in reference [37]; grid independency was tested by both doubling and halving the number of cells. The transport phenomena of liquid water between the different mesh systems were almost the same. The difference in results for the different mesh systems was so small that it is negligible.

3. Results and discussion

In order to investigate two-phase flow behaviour across the GDL, three different cases corresponding to different static contact angles of GDL and catalyst layer were simulated as listed in Table 1. As shown in Fig. 4a, Case 1 considered the GDL (the surrounding surfaces of the small holes and the surfaces on both ends of the small holes) as hydrophilic (static contact angle of 45°), Case 2 considered the GDL as hydrophobic (static contact angle of 135°), Case 3 considered the cathode electrode (all the surfaces of the GDL and the catalyst layer) as hydrophobic (static contact angle of 135°). A liquid water film was initially placed

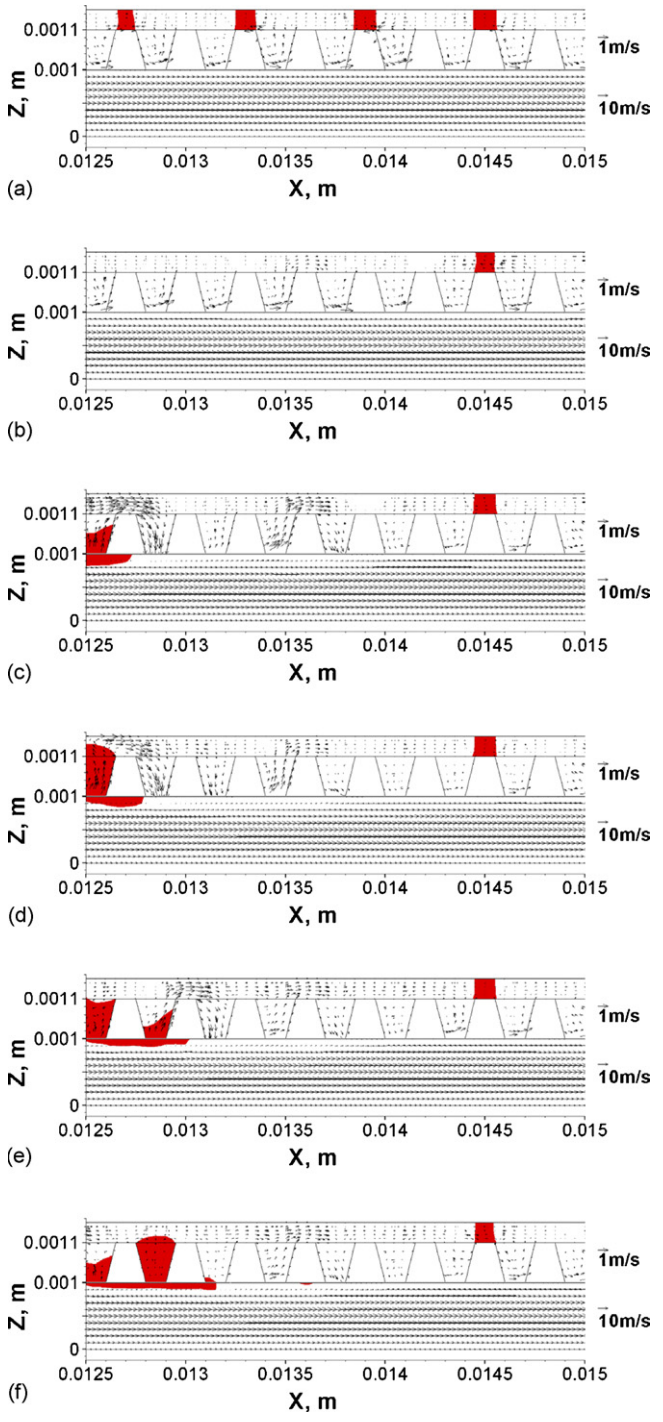

Fig. 7. Water distribution and velocity field on the center-plane ($y = 0.0005$ m) in outlet section for Case 1 (×2 magnification along the z-direction for the electrode, ×3 minification along the z-direction for the flow channel) ((a) $t = 0.01$ s; (b) $t = 0.016$ s; (c) $t = 0.019$ s; (d) $t = 0.0192$ s; (e) $t = 0.0195$ s; (f) $t = 0.02$ s).

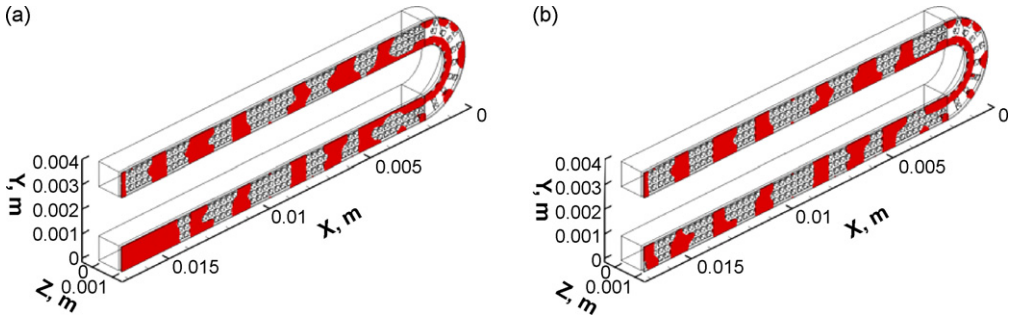

Fig. 8. Liquid water distribution in 3D view for Case 2 ((a) $t = 0.005$ s; (b) $t = 0.02$ s).

on the catalyst layer for all the three cases to investigate the water removal characteristics. Fig. 4b shows the arrangement of the initial water distribution, the "red colouring" represents liquid water. Detailed results and discussions are given below.

3.1. Case 1: water films with a thickness of 0.03 mm placed on catalyst layer with hydrophilic GDL

The first case was simulated to investigate the effects of the hydrophilic GDL on liquid water flow behaviour. As shown in Fig. 4, and listed in Table 1, water films with a thickness of 0.03 mm were placed on catalyst layer with hydrophilic GDL. Rupture of water films, and water transport across the GDL were studied.

3.1.1. Formation of liquid water "mesh"

Fig. 5 shows the liquid water distribution in 3D view. At $t = 0.0002$ s (Fig. 5a), water film started rupturing from the corner to the straight sections. Such process is similar to the results reported in reference [37], which has concluded that the process is due to the stronger secondary flow around the corner. It could also be noticed that, at $t = 0.01$ s (Fig. 5b), the initially set liquid water film ruptured into liquid water "mesh". As time passed, more parts of the "mesh" ruptured (Fig. 5c and d). However, most of the liquid water "mesh" remained until $t = 0.02$ s (Fig. 5d). The reason that such liquid water "mesh" formed could be explained with help of Fig. 6, which shows the cross-section at $x = 0.00805$ m in the lower section (outlet) of the computation domain. At $t = 0.001$ s (Fig. 6a), the initially attached flat water film was in wave-form, and then, at $t = 0.0015$ s (Fig. 6b), more air started flowing into the electrode and the water film was broken up. After a period of time, at $t = 0.002$ s (Fig. 6c), liquid water were broken up into four parts—between the holes of the GDL, and the two sides of the holes. Therefore, as shown in Figs. 5 and 6, the liquid water "mesh" had its void area directly facing the holes, and its liquid water surrounding the holes. Later on, these parts of water did not

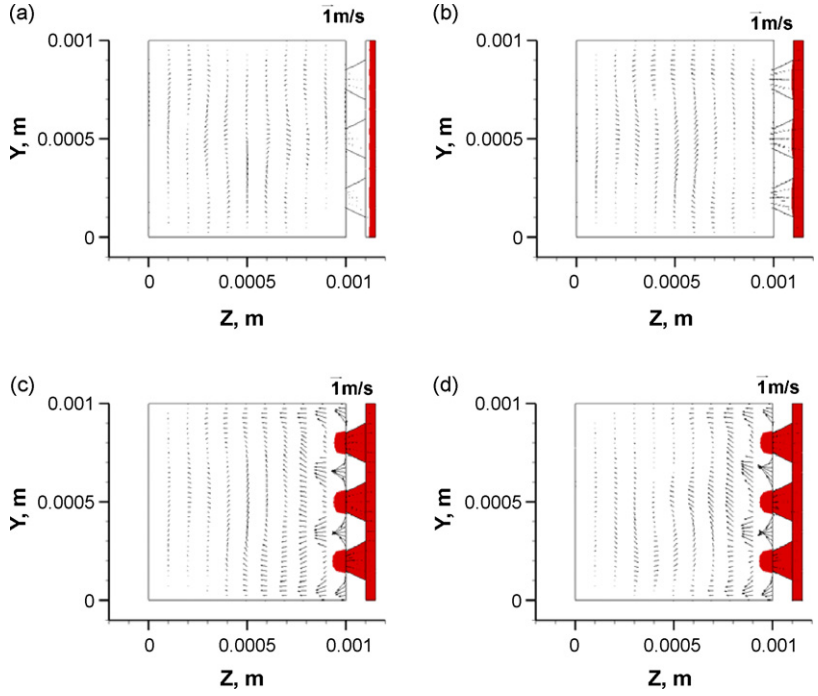

Fig. 9. Water distribution and velocity field on the plane at $x = 0.00805$ m in outlet section for Case 2 ((a) $t = 0.001$ s; (b) $t = 0.002$ s; (c) $t = 0.005$ s; (d) $t = 0.02$ s).

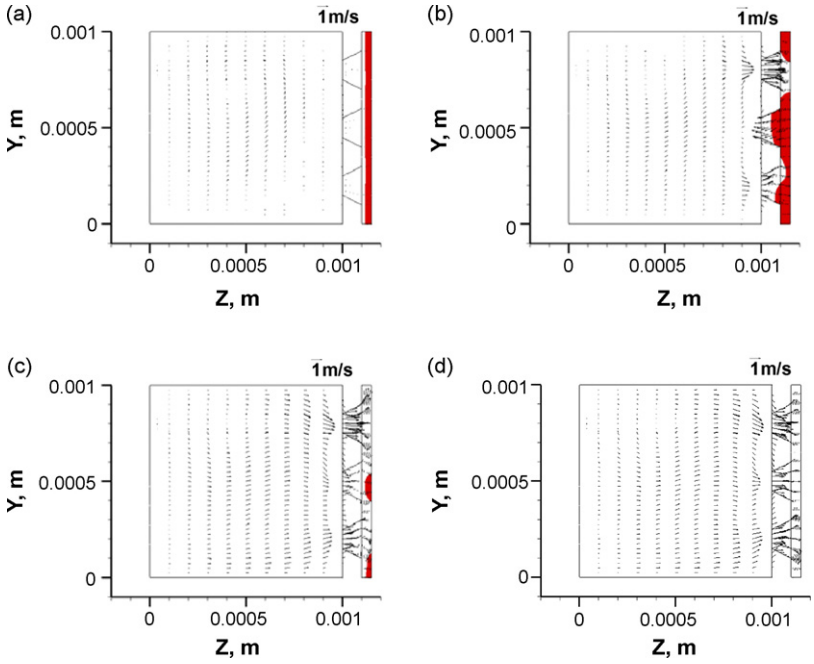

Fig. 10. Water distribution and velocity field on the plane at $x = 0.01405$ m in outlet section for Case 2 ((a) $t = 0.004$ s; (b) $t = 0.0047$ s; (c) $t = 0.0049$ s; (d) $t = 0.005$ s).

move to anywhere else (Fig. 6d). This is because these parts of water were sticking on both the surface of the catalyst layer and the bottom surface of the GDL. However, it has been concluded in reference [37], this GDL has significant effect on breaking up liquid water between the holes. The reason that such effect was not observed in this case is due to the hydrophilic property of the GDL. As mentioned, these parts of water also stick on the surface of the GDL, which provided strong wall adhesion. Therefore, the liquid water became harder to be removed. However, some parts of the liquid water "mesh" could still be broken up, as shown in Fig. 5. Fig. 7a and b shows a clear view on such process, it could be observed that some parts of the liquid water between the holes were removed. Based on the water flow behaviours that described in this section, it could be concluded that, hydrophilic GDL could provide more significant wall adhesion effect on liquid water in catalyst layer, thus preventing liquid water flowing out, which is not good for PEM fuel cell operation.

3.1.2. Back flow of liquid water

Even liquid water "mesh" was formed in the catalyst layer, some liquid water still flowed out of the electrode. Fig. 7 shows the center plane ($y = 0.0005$ m) of the lower straight section. At $t = 0.019$ s (Fig. 7c), some liquid water from upstream could be observed. It should be noticed that, the coming water did not leave the surface of the GDL. This is because of the strong wall adhesion of GDL surface. As water flowed along the GDL surface, when it reached the holes of the GDL, due to the strong wall adhesion, some of the water flowed along the surface of the GDL into the holes, as shown in Fig. 7. When one of the holes was filled with water (Fig. 7e), other liquid water could then "jump" that hole to the next, and similar liquid water flow behaviours could be observed in the next hole—some water flowed in, some water "jumped". As shown in Fig. 7d–f, some of the water flowed across the GDL into the catalyst layer, and then flowed out again across the next hole. As mentioned, the main reason that such flow phenomenon was observed is due to the hydrophilic property of the GDL (strong wall adhesion). Even some of the water could be removed from the electrode; however, water could not leave the surface of the GDL. Such process increased the chance for the liquid water flowing back into the electrode, and such back flow of liquid water is not good for PEM fuel cell operation—it blocks the GDL and the catalyst layer.

3.2. Case 2: water films with a thickness of 0.03 mm placed on catalyst layer with hydrophobic GDL

The second case was simulated to investigate the effects of the hydrophobic GDL on liquid water flow behaviour. As shown in Fig. 4, and listed in Table 1, water films with a thickness of 0.03 mm were placed on catalyst layer with hydrophobic GDL. Rupture of water films, and water transport across the GDL were studied.

3.2.1. Rupture of liquid water film

As shown in Fig. 8, the liquid water film ruptured into different pieces. The void and flooding areas were clearly separated. Liquid water occupied both the area under the holes and between the holes of the GDL, this is dissimilar to Case 1, in which most water stayed between the holes and formed "mesh". Figs. 9 and 10 show the water distribution and velocity field on the y–z planes for both the flooding area and void area, respectively. For the flooding area (Fig. 9), the flat water film became in wave-form first (Fig. 9a), and then, more water

flowed onto this plane, then water filled the whole catalyst layer and touched the surface of the GDL (Fig. 9b). As time passed, at $t = 0.005$ s (Fig. 9c), some water already flowed through the GDL into the gas flow channel. However, water almost stopped moving after that, at $t = 0.02$ s (Fig. 9d), the water distribution remained almost the same (by comparing to Fig. 9c). This is because both the air flow along the channel and the wall adhesion stopped liquid water moving. For the void area (Fig. 10), it could be observed that the water film first became in waveform as well (Fig. 10a), and then was broken up by the air flow from the holes of the GDL (Fig. 10b). Fig. 10a and b showed very similar water flow pattern as in Case 1, however, when the liquid water was split into small pieces, dissimilar to Case 1, the water were removed. This is because of the hydrophobic property of the GDL—when the small pieces of liquid water touched the surface of the GDL, the wall adhesion was weak and could not hold the water. Therefore, these small pieces of liquid water were flowed away and formed the flooding areas, as discussed with Fig. 9. Generally speaking, the whole process described with Figs. 9 and 10 produced those flooding and void areas.

3.2.2. *Force balance across the GDL*

As discussed in Case 1, there were small pieces of the liquid water staying between the holes of the GDL, but such phenomenon was not observed in Case 2 due to the weak wall adhesion of the GDL surface. However, the weak wall adhesion could be enhanced by increasing the contact area between GDL surface and liquid water. Fig. 11 shows the water distribution and velocity field on the center-plane ($y = 0.0005$ m) in the lower section, it could be observed that the initial water film was broken up, and both the void and flooding areas were formed. As discussed in Section 3.2.1, after these flooding areas were formed, the water almost stopped moving. This is because as the flooding area increased, the contact area between water and electrode surface also increased, so the wall adhesion increased. When the flooding area was large enough, the wall adhesion became strong enough to stop liquid water moving. Unfortu-

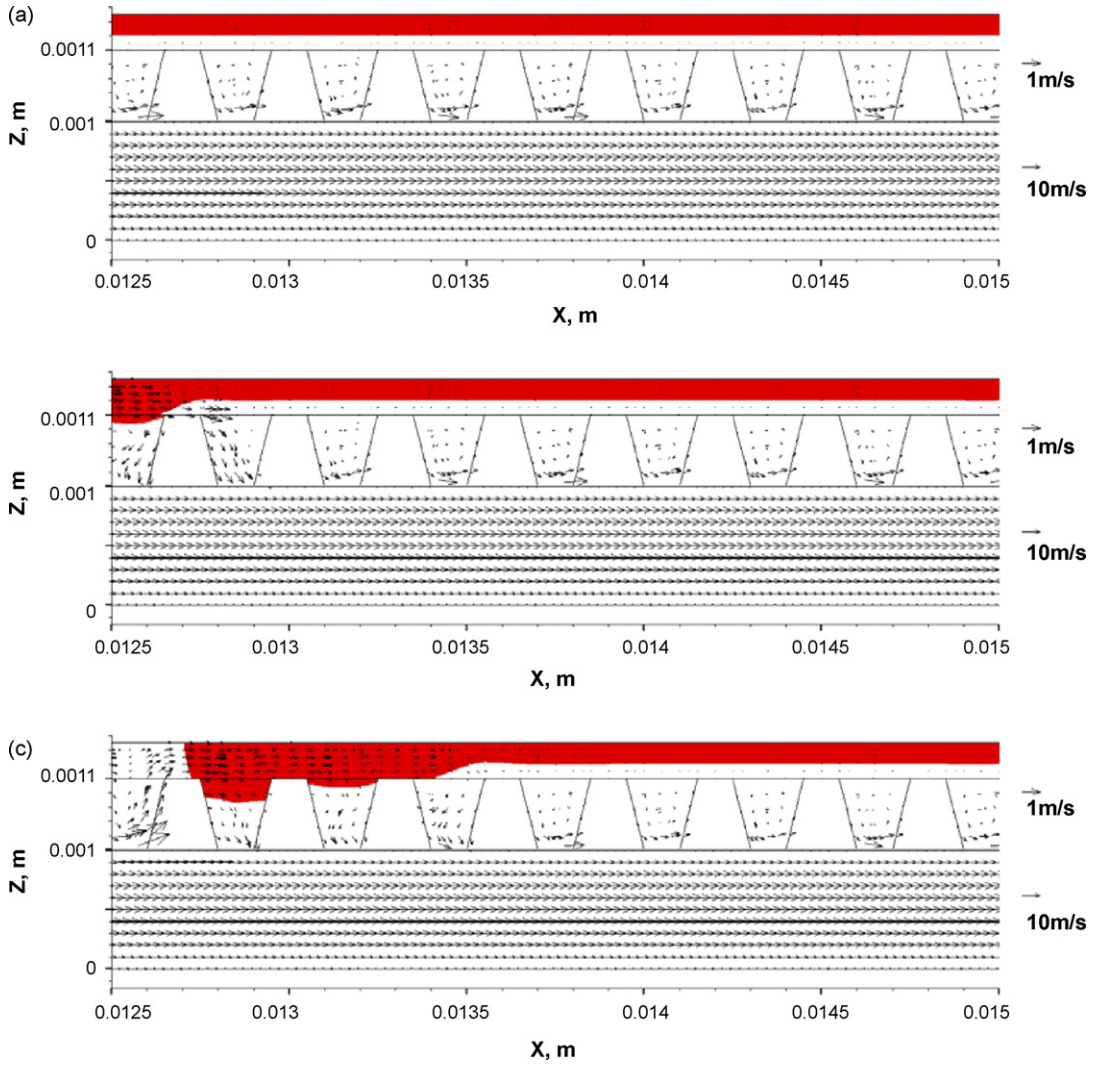

Fig. 11. Water distribution and velocity field on the center-plane ($y = 0.0005$ m) in outlet section for Case 2 ($\times 2$ magnification along the z-direction for the electrode, $\times 3$ minification along the z-direction for the flow channel) ((a) $t = 0.002$ s; (b) $t = 0.003$ s; (c) $t = 0.004$ s; (d) $t = 0.005$ s; (e) $t = 0.006$ s; (f) $t = 0.02$ s).

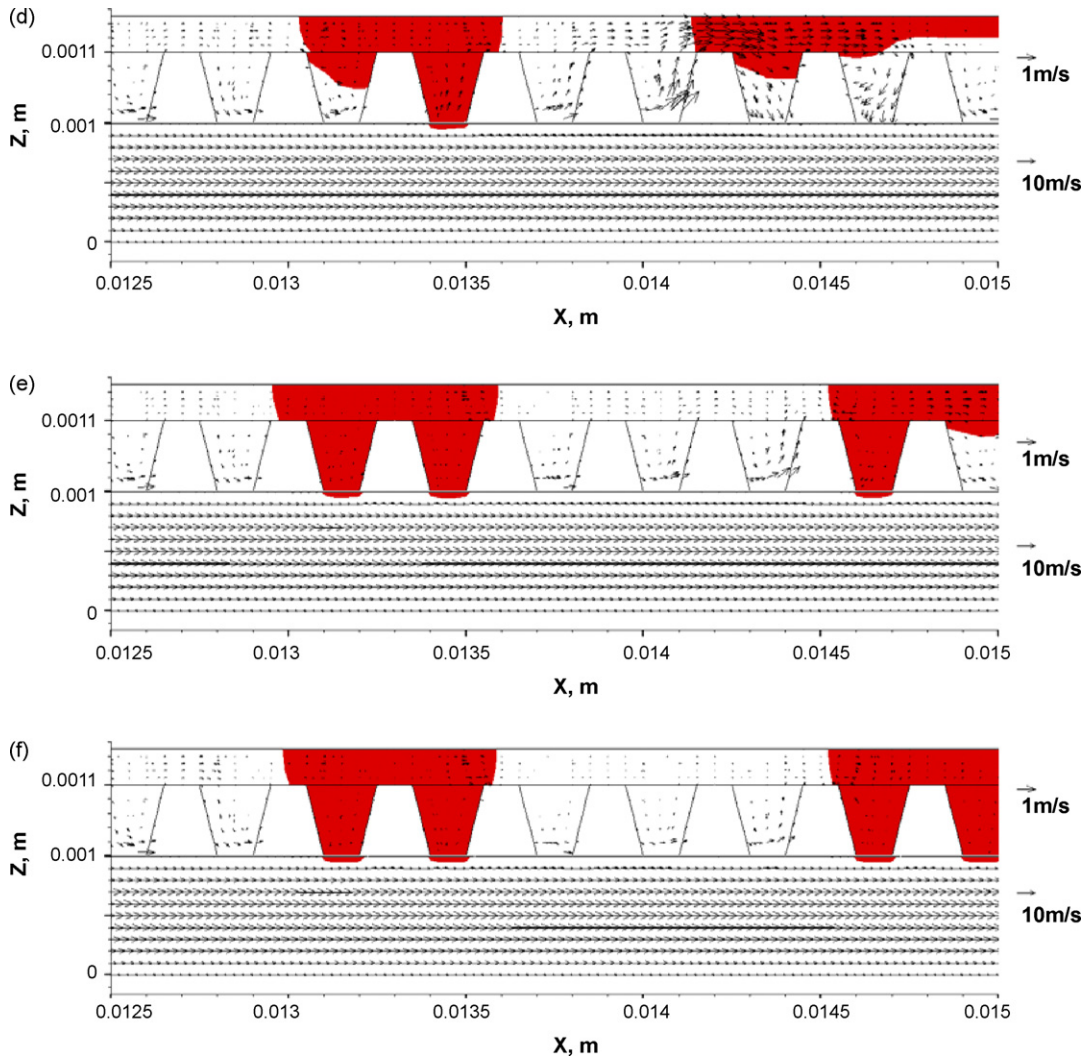

Fig. 11. (*Continued*).

nately, based on the water flow phenomenon described in this section, even the GDL was changed to be hydrophobic, the water removal was still not improved, a significantly amount of water could still be observed in the catalyst layer. Therefore, it could be concluded that, if only hydrophobic GDL is used, liquid water could be expelled to both sides (gas flow channel and catalyst layer), the catalyst layer could be flooded and the water drainage could be even worse.

3.3. Case 3: water films with a thickness of 0.03 mm placed on catalyst layer with hydrophobic electrode (GDL and catalyst layer)

The third case was simulated to investigate the effects of the combination of hydrophobic GDL and hydrophobic catalyst layer on liquid water flow behaviour. As shown in Fig. 4, and listed in Table 1, water films with a thickness of 0.03 mm

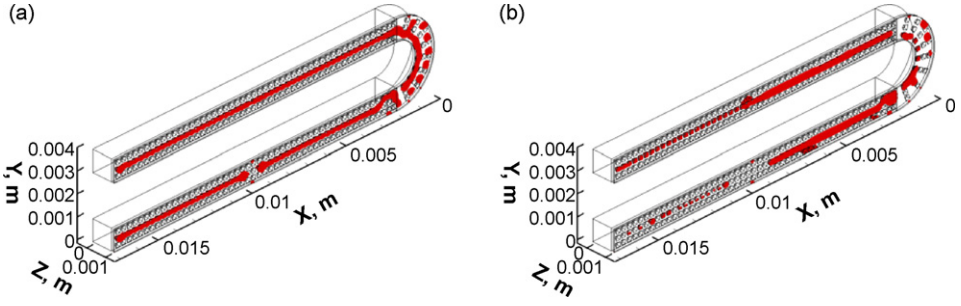

Fig. 12. Liquid water distribution in 3D view for Case 3 ((a) $t = 0.001$ s; (b) $t = 0.02$ s).

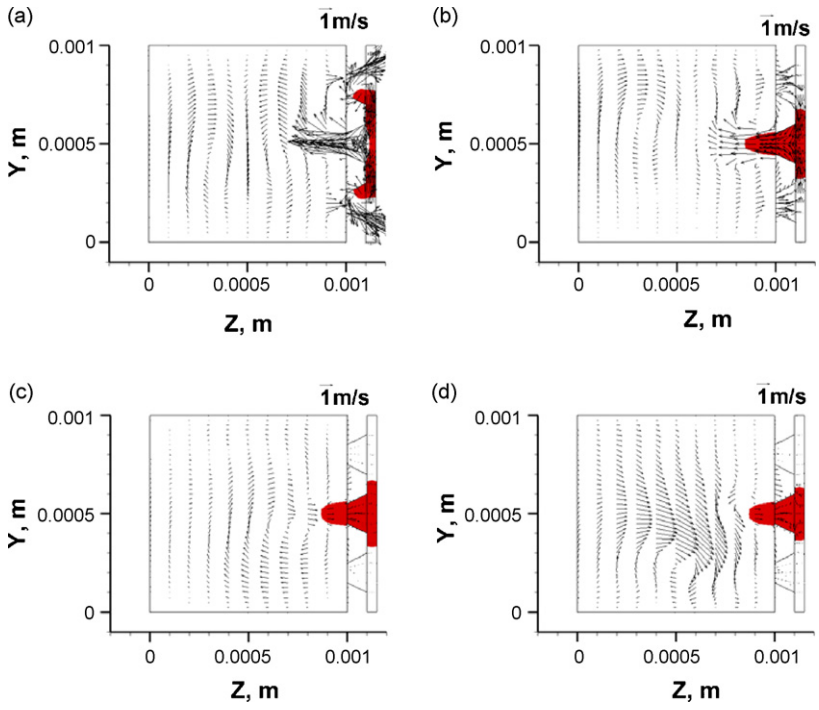

Fig. 13. Water distribution and velocity field on the plane at $x = 0.00805$ m in outlet section for Case 3 ((a) $t = 0.0003$ s; (b) $t = 0.0005$ s; (c) $t = 0.002$ s; (d) $t = 0.02$ s).

were placed on catalyst layer. Rupture of water films, and water transport across the GDL were studied.

3.3.1. Formation of liquid water "string"

Fig. 12 shows the liquid water distribution in 3D view for Case 3. It could be observed that the water distribution was different from the previous cases. At $t = 0.001$ s (Fig. 12a), liquid water "strings" were formed along the center line of the main air flow. The water "strings" then started being removed, as shown in Fig. 12b, at $t = 0.02$ s, some parts of the water "strings" were already removed. The reason that the water "strings" were formed could be explained with help of Fig. 13, which shows the water distribution and velocity field on the plane at $x = 0.00805$ m in the lower section. At $t = 0.0003$ s (Fig. 13a), air flowed into the holes on both sides, and pushed liquid water to the middle, and due to the weak wall adhesion of all the surfaces of the electrode, water became easier to be removed. Therefore, liquid water followed the air stream and flowed from the top and bottom into the hole in the middle. At $t = 0.002$ s (Fig. 13c), the movement of water became slower, this is because once the "strings" being formed, the air flowing into the top and bottom holes could also flow out from other top and bottom holes, thus decreasing the driving force of the liquid water in the middle, however, as mentioned, water was still being removed.

3.3.2. Liquid water flowing back into the electrode

Fig. 14 shows the water distribution and velocity field on the center-plane of the lower section ($y = 0.0005$ m), the formation of "strings" could also be observed from this figure. At $t = 0.0003$ s (Fig. 14a), strong streams flowing out of the electrode could be observed, and later on, more water flowed onto this plane (as mentioned, from the top and bottom), at $t = 0.0004$ s (Fig. 14b), the whole electrode was filled with water and the water was still flowing out. The stream became weaker at $t = 0.0007$ s (Fig. 14d), and at that time, more water could be observed in the gas flow channel. At $t = 0.001$ s (Fig. 14e), the streams flowing back into the electrode could be observed, and some water that previously moved into the gas flow channel then moved back into the electrode. As shown in Fig. 14f, at $t = 0.002$ s, less water could be observed in the gas flow channel, and the streams across the holes could be no longer apparently observed. The reason that some water flowed into the gas flow channel but then flowed back into the electrode is that, from the beginning the driving force to flow out the water was strong, however, after the "strings" were formed, the driving force was lost because the air stream could flow out from other holes, and part of the water that just flowed into the gas flow channel could flow back into the electrode.

3.3.3. "Splashing" of liquid water

Fig. 15 shows the water distribution and velocity field on the center-plane of the lower section ($y = 0.0005$ m) for a later time period. At $t = 0.009$ s, some water from the upstream could be observed, the water flowed along the air stream and splashed on to the holes at the downstream. Some water inside the holes was taken away by the liquid water "splashing" process. As shown in Fig. 15c ($t = 0.012$ s), when water flowed away from the hole, significant amount of water in the electrode was removed. Later on, another part of water from the upstream could be observed, and more water was taken away by it, as shown in Fig. 15d–f. As discussed in Case 1, dissimilar to this case, due to the hydrophilic property of the GDL, liquid water flowing from the upstream would always stick on the surface of the GDL and even flow back into the electrode. However, in this case, the wall adhesion is weaker due to the hydrophobic property of the whole electrode.

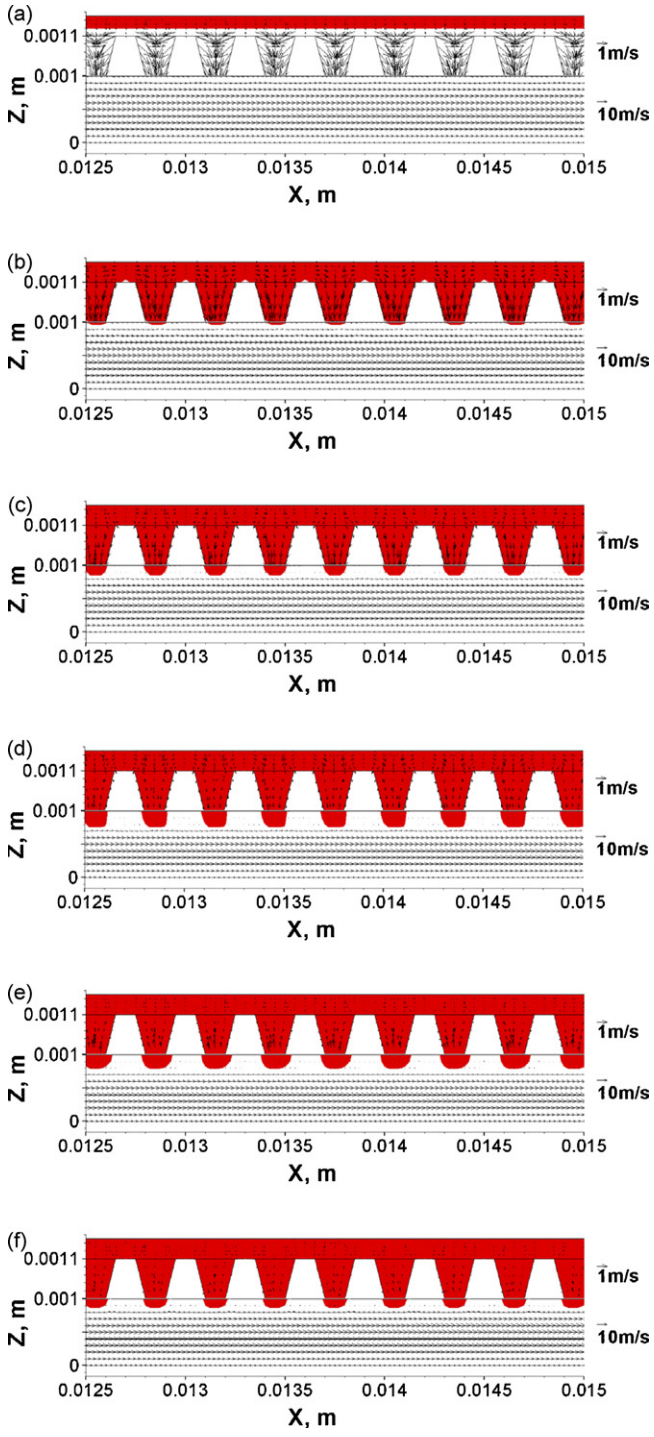

Fig. 14. Water distribution and velocity field on the center-plane ($y = 0.0005$ m) in outlet section for Case 3 ($\times 2$ magnification along the z-direction for the electrode, $\times 3$ minification along the z-direction for the flow channel) ((a) $t = 0.0003$ s; (b) $t = 0.0004$ s; (c) $t = 0.0005$ s; (d) $t = 0.0007$ s; (e) $t = 0.001$ s; (f) $t = 0.002$ s).

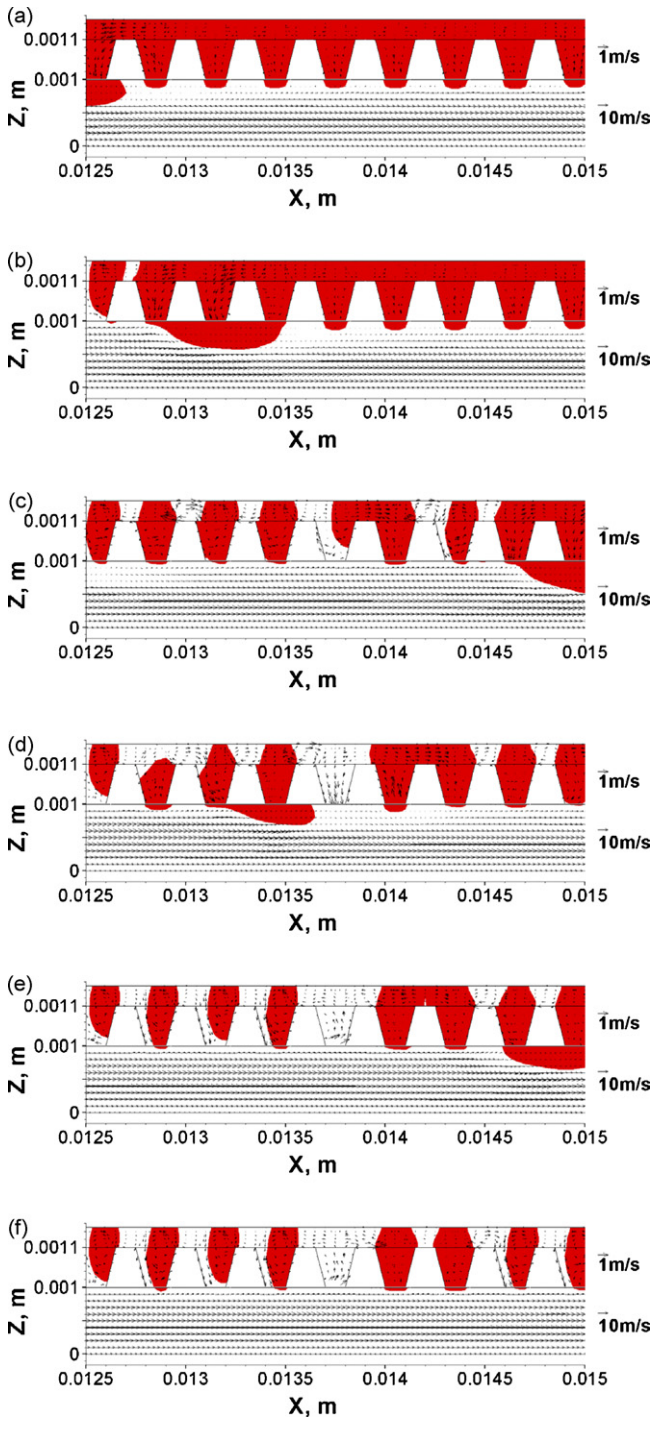

Fig. 15. Water distribution and velocity field on the center-plane ($y = 0.0005$ m) in outlet section for Case 3 ($\times 2$ magnification along the z-direction for the electrode, $\times 3$ minification along the z-direction for the flow channel) ((a) $t = 0.009$ s; (b) $t = 0.01$ s; (c) $t = 0.012$ s; (d) $t = 0.013$ s; (e) $t = 0.014$ s; (f) $t = 0.015$ s).

Therefore, liquid water on the GDL surface could be flowed away more easily, and the "splashing" of water could take some water away from the electrode, which is good for PEM fuel cell operation. Based on the flow behaviours that described in this section, it could be concluded that, the hydrophobic level of the electrode must be carefully controlled, and the catalyst layer must have higher or equal hydrophobic level by comparing to the GDL. So that liquid water could be expelled in one direction (from catalyst layer to GDL).

3.4. Comparison of water amount variations

Fig. 16 shows the comparison of water amount variations inside the electrode for the three cases. In reference [37], the

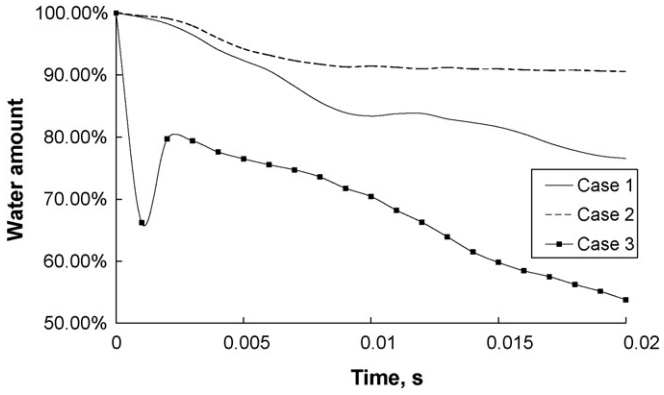

Fig. 16. Water amount variation inside the electrode for the three cases.

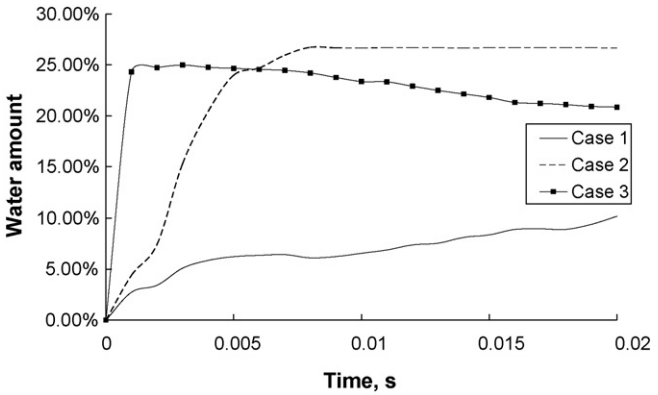

Fig. 18. Water amount variation inside the GDL for the three cases.

same case with a contact angle of 90° for all the electrode surfaces was simulated, it showed that at $t = 0.02$ s, the water amount inside the electrode became 88%. For Case 1, surprisingly, a hydrophilic GDL even improved the water removal ability (77% at $t = 0.02$ s). This is because such GDL helped break up the water film into small pieces, and the small pieces of water could be more easily removed. For Case 2, a hydrophobic GDL did not provide any improvements on water removal (90% at $t = 0.02$ s), this is because such GDL provided more chances to form large pieces of water, therefore, the increased contact area between the electrode surface and water increased the wall adhesion to stop liquid water moving. Case 3 showed significant advantage in water removal by comparing to the other two cases (54% at $t = 0.02$ s). The reason is that, the hydrophobic catalyst layer helped break up the liquid water film, and the hydrophobic GDL helped water flow out of the electrode. An increase of water amount could be observed following a sharp drop, the reason is discussed in Section 3.3.2. Fig. 17 shows the comparison of water amount variation inside the catalyst layer for the three cases. Case 3 still provided a much better result than the other two cases. However, Case 2 showed less water amount by comparing to Case 1, as mentioned in section 3.2, this is because the large pieces of liquid water in Case 2 occupied both the GDL and the electrode. Fig. 18 shows the comparison of water amount variation inside the GDL, without any surprise, Case 2 showed more water amount than Case 1. Base on the comparison of water amount variation of the three cases, it could be concluded that, if all the surfaces of the electrode are hydrophobic, water removal could be significantly improved, and only changing the wettability of the GDL might not provide any significant improvement on water removal. The hydrophobic level of the electrode must be carefully controlled, and the catalyst layer must have higher or equal hydrophobic level by comparing to the GDL. So that liquid water could be expelled in one direction (from catalyst layer to GDL). As mentioned in Section 4.3 of reference [1], it was also stated that: when people prepare the catalyst layer, PTFE is often added also, because the hydrophobic PTFE will expel the product water to other places, this also supports the author's conclusion.

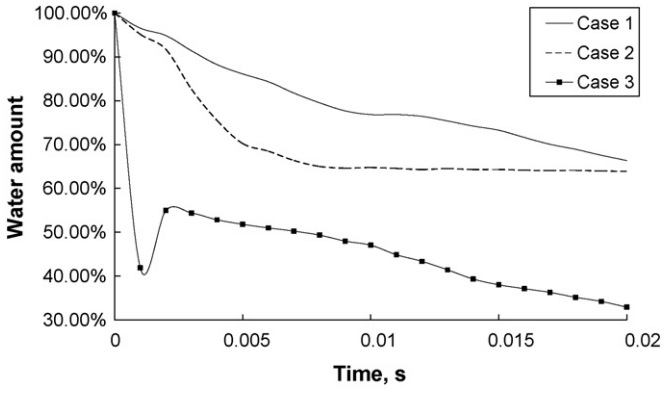

Fig. 17. Water amount variation inside the catalyst layer for the three cases.

4. Conclusions

In this paper, a cathode electrode with different wettabilities have been proposed and investigated. The liquid water behaviours in the electrode together with serpentine gas flow channel on cathode side of a PEM fuel cell were studied by employing a 3D, unsteady, two-phase flow model in FLUENT with an initial water distribution. By investigating the flow behaviours of liquid water and air velocity fields, the following water management issues and suggestions are given:

(1) Hydrophilic GDL could retain liquid water on its surfaces, and liquid water "mesh" could be formed in catalyst layer along the surfaces of the GDL. These hydrophilic surfaces result in stronger wall adhesions, so it is difficult for water to be removed, which is not good for PEM fuel cell operation.
(2) Hydrophilic GDL surface could also attract liquid water from gas flow channel into the electrode, which is not good for PEM fuel cell operation.
(3) If only hydrophobic GDL is used, liquid water could be expelled to both sides (gas flow channel and catalyst layer), the catalyst layer could be flooded and the water drainage could be even worse.
(4) Hydrophobic catalyst layer could help break up liquid water films significantly. Liquid water "strings" could be formed, the water drainage could also be improved.

(5) If liquid water from the electrode moves too fast into the gas flow channel, part of the water could be "pushed" back into the electrode due to the air flow.
(6) Due to the weak wall adhesion of hydrophobic GDL surfaces, liquid water from gas flow channel could take away some liquid water inside the GDL, and such "splashing" of liquid water is good for water drainage.
(7) The hydrophobic level of the electrode must be carefully controlled, and the catalyst layer must have higher or equal hydrophobic level by comparing to the GDL. So that liquid water could be expelled in one direction (from catalyst layer to GDL).

Acknowledgements

The authors are grateful for the support of this work by the Auto21^{TM} Networks of Centres of Excellence (Grant D07-DFC), the Natural Sciences and Engineering Research Council of Canada (NSERC), the Canada Foundation for Innovation (CFI), the Ontario Innovation Trust (OIT), and the Graduate School at the University of Windsor.

References

[1] J. Larminie, A. Dicks, Fuel Cell Systems Explained, second ed., John Wiley & Sons, New York, 2000.
[2] J.S. Yi, J.D. Yang, C. King, AIChE J. 50 (2004) 2594.
[3] C.Y. Wang, Chem. Rev. 104 (2004) 4727.
[4] A. Kraytsberg, Y. Ein-Eli, J. Power Sources 160 (2006) 194.
[5] S. Um, C.Y. Wang, K.S. Chen, J. Electrochem. Soc. 147 (2000) 4485.
[6] S. Dutta, S. Shimpalee, J.W. Van Zee, J. Appl. Electrochem. 30 (2000) 135.
[7] E. Hontanon, M.J. Escudero, C. Bautista, P.L. Garcia-Ybarra, L. Daza, J. Power Sources 86 (2000) 363.
[8] S.W. Cha, R. O'Hayre, Y. Saito, F.B. Prinz, J. Power Sources 134 (2004) 57.
[9] A.A. Kulikovsky, Electrochem. Commun. 3 (2001) 460.
[10] Z.H. Wang, C.Y. Wang, K.S. Chen, J. Power Sources 94 (2001) 40.
[11] L. You, H. Liu, Int. J. Heat Mass Transfer 45 (2002) 2277.
[12] W. He, J.S. Yi, T.V. Nguyen, AIChE J. 46 (2000) 2053.
[13] L.B. Wang, N.I. Wakayama, T. Okada, Electrochem. Commun. 4 (2002) 584.
[14] B. Carnes, N. Djilali, Electrochem. Acta 52 (2006) 1038.
[15] C.I. Lee, H.S. Chu, J. Power Sources 161 (2006) 949.
[16] H. Meng, J. Power Sources 168 (2007) 218.
[17] U. Pasaogullari, C.Y. Wang, J. Electrochem. Soc. 152 (2005) A380.
[18] H. Meng, C.Y. Wang, J. Electrochem. Soc. 152 (2005) A1733.
[19] Y. Wang, C.Y. Wang, J. Electrochem. Soc. 153 (2006) A1193.
[20] H. Meng, C.Y. Wang, Chem. Eng. Sci. 59 (2004) 3331.
[21] H. Ju, C.Y. Wang, J. Electrochem. Soc. 151 (2004) A1954.
[22] H. Ju, C.Y. Wang, S. Cleghorn, U. Beuscher, J. Electrochem. Soc. 153 (2006) A249.
[23] Y. Wang, C.Y. Wang, J. Power Sources 153 (2006) 130.
[24] P. Quan, B. Zhou, A. Sobiesiak, Z. Liu, J. Power Sources 152 (2006) 131.
[25] K. Jiao, B. Zhou, P. Quan, J. Power Sources 154 (2006) 124.
[26] K. Jiao, B. Zhou, P. Quan, J. Power Sources 157 (2006) 226.
[27] T.V. Nguyen, M.W. Knobbe, J. Power Sources 114 (2003) 70.
[28] T.A. Trabold, J.P. Owejan, D.L. Jacobson, M. Arif, P.R. Huffman, Int. J. Heat Mass Transfer 49 (2006) 4712.
[29] X. Li, I. Sabir, J. Park, J. Power Sources 163 (2007) 933.
[30] D. Spernjak, A.K. Prasad, S.G. Advani, J. Power Sources 170 (2007) 334.
[31] X.G. Yang, F.Y. Zhang, A. Lubawy, C.Y. Wang, Electrochem. Solid-State Lett. 7 (2004) A408.
[32] F.Y. Zhang, X.G. Yang, C.Y. Wang, J. Electrochem. Soc. 153 (2006) A225.
[33] J.H. Nam, M. Kaviany, Int. J. Heat Mass Transfer 46 (2003) 4595.
[34] H. Dohle, R. Jung, N. Kimiaie, J. Mergel, M. Muller, J. Power Sources 124 (2003) 371.
[35] U. Pasaogullari, C. Wang, Electrochem. Acta 49 (2004) 4359.
[36] S. Freni, G. Maggio, E. Passalacqua, Mater. Chem. Phys. 48 (1997) 199.
[37] K. Jiao, B. Zhou, J. Power Sources 169 (2007) 296.
[38] Fluent 6.2 User's Guide, Fluent Inc., 2005.